International Journal of Heat and Fluid Flow 32 (2011) 1083–1097

Contents lists available at SciVerse ScienceDirect

International Journal of Heat and Fluid Flow

journal homepage: www.elsevier.com/locate/ijhff

The influence of pipe length on thermal statistics computed from DNS of turbulent heat transfer

S. Saha [a,*], C. Chin [a], H.M. Blackburn [b], A.S.H. Ooi [a]

[a] Department of Mechanical Engineering, University of Melbourne, Victoria 3010, Australia
[b] Department of Mechanical and Aerospace Engineering, Monash University, Victoria 3800, Australia

ARTICLE INFO

Article history:
Received 27 June 2011
Received in revised form 31 August 2011
Accepted 10 September 2011
Available online 5 October 2011

Keywords:
Turbulent heat transfer
Direct numerical simulation
Pipe flow
Prandtl number

ABSTRACT

We present results from direct numerical simulation of turbulent heat transfer in pipe flow at a bulk flow Reynolds number of 5000 and Prandtl numbers ranging from 0.025 to 2.0 in order to examine the effect of streamwise pipe length ($\pi\delta \equiv \pi D/2 \leqslant L \leqslant 12\pi\delta$) on the convergence of thermal turbulence statistics. Various lower and higher order thermal statistics such as mean temperature, rms of fluctuating temperature, turbulent heat fluxes, two-point auto and cross-correlations, skewness and flatness were computed and it is found that the value of L required for convergence of the statistics depends on the Prandtl number: larger Prandtl numbers requires comparatively shorter pipe length for convergence of most of the thermal statistics.

1. Introduction

Within the last decade, simulation procedures based on computational fluid dynamics (CFD) have become an essential design and analysis tool in a wide and ever-increasing range of applications involving fluid flow and heat transfer. Direct numerical simulation (DNS) is a well-accepted numerical tool among the most popular branches of CFD for high-fidelity solution of turbulent flows. From the time-dependent velocity and scalar fields obtained from DNS, a huge range of information such as single- and multi-point statistics can be readily calculated. This information is particularly useful when research demands accurate analysis of quantities that are difficult to measure experimentally, such as velocity and pressure gradients. Additional details from DNS have complemented existing experimental data and contributed significantly to the understanding of turbulence physics, and to the improvement of lower-order models.

Since the first successful DNS of turbulent channel flow and heat transfer at $Re_\tau = u_\tau\delta/\nu \approx 180$ (where u_τ is the friction velocity, δ is the half channel height or pipe radius, ν is the kinematic viscosity) for $Pr = \nu/\alpha = 0.1$, 0.71 and 2.0 (where α is the thermal diffusivity) by Kim and Moin (1989), many researchers have used DNS data to gain significant insight into the physics wall-bounded turbulent flow and heat transfer. Most of these simulations were performed for turbulent heat transfer in channel flow over a wide range of Reynolds numbers as well as Prandtl numbers with various configurations of thermal boundary conditions. By comparison, only a relatively limited number of DNS studies for turbulent heat transfer in non-buoyant pipe flow may be found in the literature as can be seen from an examination of Table 1. Typically if Prandtl number variations were examined, Re_τ had been comparatively low and conversely Prandtl number was often fixed (typically at $Pr = 0.71$, the value for air) if Re_τ variations were examined.

In the majority of these DNS studies the flow is assumed to be fully developed and hence it is justified to assume streamwise periodicity. However, other studies found that turbulence statistics may be affected by the length of the computational domain because large-scale streamwise structures, sometimes referred to as the "large-scale motions" (LSMs) may extend further than the streamwise periodic length. If the computational domain is too short, then the LSM can be "contaminated" by the enforced streamwise periodicity of the boundary conditions. If too long, then there is a wastage of computational resources. Hence, it is important to find the optimum length of the computational domain and to understand the effects on the DNS data that may result if simulations were conducted in a domain of insufficient length.

It was experimentally observed that the interaction between the outer layer and the inner layer in wall-bounded turbulent flow increased with increasing Reynolds number (Naguib and Wark, 1992). Kim and Adrian (1999) in their studies explained that very large-scale motions (VLSMs) in flat-plate boundary layers were much longer than LSMs appeared in the outer layer of a turbulent pipe flow. Monty et al. (2007) reported that the length of these long meandering structures in pipe and channel flows was up to 25δ.

* Corresponding author. Tel.: +61 3 8344 6748; fax: +61 3 8344 4290.
E-mail address: sumons@student.unimelb.edu.au (S. Saha).

0142-727X/$ - see front matter © 2011 Elsevier Inc. All rights reserved.
doi:10.1016/j.ijheatfluidflow.2011.09.003

Table 1
Overview of turbulent heat transfer in wall-bounded flows.

Previous DNS	Re_τ	Pr	Boundary conditions
Channel flows			
Kim and Moin (1989)	180	[0.1, 0.71, 2.0]	UHG[1], UTD[2], PF[9]
Lyons et al. (1991)	150	1.0	UTD[2], CF[10]
Kasagi et al. (1992)	150	0.71	MBC[3], PF[9]
Kasagi and Ohtsubo (1993)	150	0.025	MBC[3], PF[9]
Kawamura et al. (1997)	180	[0.025, 0.05, 0.1, 0.2, 0.4, 0.6, 0.71, 1.0, 1.5, 5.0]	MBC[3], PF[9]
Abe et al. (1998)	[180, 395]	[(0.025, 0.1, 0.2, 0.4, 0.71, 5.0), (0.025, 0.2, 0.71)]	MBC[3], PF[9]
Matsubara et al. (1998)	150	[0.1, 0.3, 0.71, 1.5]	SMTG[4], PF[9]
Kawamura et al. (1998a)	180	[0.025, 0.05, 0.1, 0.2, 0.4, 0.6, 5.0]	MBC[3], PF[9]
Kawamura et al. (1998b)	180	[0.025, 0.05, 0.1, 0.2, 0.4, 0.6, 0.71, 1.0, 1.5, 5.0]	MBC[3], PF[9]
Kawamoto and Kawamura (1998)	180	[0.025, 0.05, 0.4, 0.71]	SMTG[4], PF[9]
Kawamoto and Kawamura (1999a)	180	[0.025, 0.71]	UTD[2], MBC[3], PF[9]
Kawamoto and Kawamura (1999b)	[180, 395]	[(0.025, 0.05, 0.1, 0.2, 0.4, 0.6, 5.0), (0.025, 0.2, 0.71)]	MBC[3], PF[9]
Kawamura et al. (1999)	[180, 395]	[0.025, 0.2, 0.71]	MBC[3], PF[9]
Matsubara et al. (1999)	150	0.71	SMTG[4], PF[9]
Johansson and Wikström (1999)	265	0.71	UTD[2], PF[9]
Na et al. (1999)	150	[0.3, 1.0, 3.0, 10.0]	UTD[2], PF[9]
Na and Hanratty (2000)	150	[1.0, 3.0, 10.0]	UTD[2], PF[9]
Kawamura et al. (2000)	[180, 395]	[(0.025, 0.2, 0.71, 1.0), (0.025, 0.2, 0.71, 1.0)]	UTD[2], MBC[3], PF[9], CF[10]
Kawamura and Ogawa (2001)	180	0.71	UTD[2], SMTG[4], CWTDSMTG[5], PF[9]
Matsubara et al. (2001)	150	0.71	MBC[3], SMTG[4], PF[9]
Piller et al. (2002)	150	[0.025, 0.05, 0.1, 0.3, 1.0]	UTD[2], PF[9]
Kawamura and Abe (2002)	[180, 395, 640]	[0.025, 0.71]	MBC[3], PF[9]
Abe and Kawamura (2002)	[180, 395, 640]	[0.025, 0.71]	MBC[3], PF[9]
Seki et al. (2003a)	[180, 395]	0.71	UTD[2], MBC[3], PF[9]
Seki et al. (2003b)	180	0.71	UTD[2], MBC[3], CWTDSMTG[5], PF[9]
Abe et al. (2004)	[180, 395, 640, 1020]	[0.025, 0.71]	MBC[3], PF[9]
Tsukahara et al. (2004)	[64, 70, 80, 110, 150, 180]	0.71	MBC[3], PF[9]
Kawamura et al. (2004)	[180, 395, 640, 1020]	[0.025, 0.71]	MBC[3], PF[9]
Seki and Kawamura (2004a)	180	0.71	SVTBC[6], PF[9]
Seki and Kawamura (2004b)	180	0.71	UTD[2], MBC[3], CWTDSMTG[5], PF[9]
Seki and Kawamura (2005)	180	0.71	SVTBC[6], PF[9]
Seki and Kawamura (2006)	180	0.71	SVTBC[6], PF[9]
Seki et al. (2006)	180	[0.71, 1.0, 2.0, 10.0]	MBC[3], PF[9]
Abe et al. (2008)	[180, 395, 640]	0.71	MBC[3], PF[9]
Antonia et al. (2008)	[180, 395, 640, 1020]	0.71	MBC[3], PF[9]
Yamamoto et al. (2009)	[150, 1000, 2000]	5.0	UTD[2], PF[9]
Pipe flows			
Satake et al. (2000)	[150, 180, 360, 500, 1050]	0.71	MBC[3], PF[9]
Piller (2005)	180	0.71	IWT[7], IWHF[8], MBC[3], PF[9]
Redjem-Saad et al. (2007)	186	[0.026, 0.1, 0.2, 0.4, 0.71, 1.0]	MBC[3], PF[9]
Saha et al. (2010)	170	[0.026, 0.1, 0.2, 0.4, 0.71, 1.0]	MBC[3], PF[9]

[1] USG: uniform heat generation with cold isothermal walls.
[2] UTD: uniform temperature difference (constant wall temperature difference).
[3] MBC: mixed boundary condition (wall temperature is time independent and varies linearly along streamwise direction).
[4] SMTG: spanwise mean temperature gradient (time-averaged wall temperature is uniform in streamwise and wall-normal direction).
[5] CWTDSMTG: constant wall temperature difference imposed with spanwise mean temperature gradient.
[6] SVTBC: streamwise varying thermal boundary condition.
[7] IWT: ideal isothermal boundary condition (time-averaged wall temperature is uniform and constant).
[8] IWHF: ideal isoflux boundary condition (time-averaged wall temperature varies linearly along streamwise direction).
[9] PF: Poiseuille flow.
[10] CF: Couette flow.

For DNS of turbulent channel flow with passive scalar transport, Kawamura et al. (2004) inspected the very large-scale structures of temperature fluctuation for a range of Reynolds numbers and observed the existence of VLSMs in the outer region which was closely related to "temperature front" phenomenon reported by Chen and Blackwelder (1978). With decreasing Prandtl number, near-wall streak structures become more elongated, demanding longer computational domains.

Computational cost typically increases with increasing Reynolds and Prandtl numbers in order to resolve all relevant length scales in the simulation. However, in general, our results will show the length of the pipe will need to be increase with decreasing Prandtl numbers. This is because we have to consider the need to correctly capture all key dynamical features of the LSMs and VLSMs in wall-bounded flows, computational domain sizes must be chosen carefully. In wall-bounded turbulent flows, computational cost estimated by Jiménez (2003) to scale with $\sim L_x^2 L_y Re_\tau^4$. Moreover, the ratio between the largest and the smallest length scales in thermal field is roughly proportional to $Re^{3/4}Pr^{1/2}$ at higher Prandtl numbers (Tennekes and Lumley, 1972). As a result, the computational cost for a wall-bounded thermal turbulence simulation can be approximated as $\sim L_x^2 L_y Re_\tau^4 Pr^{3/2}$ (Kasagi and Iida, 1999). It is also important to consider that the most energetic small-scale structure for temperature fluctuations is found at a streamwise wavelength of $\lambda_x^+ \approx 700$ (Yamamoto et al., 2009) whereas that for velocity fluctuations has a streamwise length of $\lambda_x^+ \approx 1000$ (Marusic et al., 2010) suggesting the computational domain must use at least $l^+ \approx 1000$ in order to avoid any "contamination" by periodicity in the streamwise direction.

DNS studies for turbulent heat transfer in a channel have been carried out using a number of different boundary conditions for the flow and thermal fields: uniform heat generation with cold isothermal walls (Kim and Moin, 1989), uniform temperature difference (Kim and Moin, 1989; Yamamoto et al., 2009), mixed boundary condition (Kasagi et al., 1992; Saha et al., 2010),

spanwise mean temperature gradient (Matsubara et al., 1998, 2001), constant wall temperature difference imposed with spanwise mean temperature gradient (Kawamura and Ogawa, 2001; Seki and Kawamura, 2004b) and streamwise varying thermal boundary condition (Seki and Kawamura, 2004a, 2006). The mixed boundary condition (see e.g. Piller (2005) and Section 2.3 below for details) for both pipe and channel flow where an isoflux heat source applied on the wall surface is one of the most common thermal boundary conditions that occurs in many practical applications.

Among those previous studies listed in Table 2, it is clearly observed that the domain length used by the investigators did not change significantly with variations in Re_τ and Pr. When the flow and heat transfer was characterized by low Re_τ(= 180) and low Pr(= 0.025), the minimum domain length was taken as 6.4δ (1152 in wall units). As outlined above, the flow at higher Reynolds number should require a longer domain length than was used in the previous studies which were limited to a domain length of 12.8δ for channel flow ($Re_\tau = 1020$) and 15δ for pipe flow ($Re_\tau = 1050$). In terms of wall units, this length should be approximately 13,000 and 16,000 respectively. Only Tsukahara et al. (2004) tried to show the influence of domain length on turbulent heat transfer in channel flow for low values of Kármán numbers (Re_τ). However, their results failed to provide any significant conclusion of selecting appropriate domain length based on variable thermal scales as a function of Pr.

The minimum length required for the computational domain is clearly dependent on both the Kármán and Prandtl numbers as these have a direct influence on turbulent flow and heat transfer characteristics in pipe flow. Satake et al. (2000) and Redjem-Saad et al. (2007) carried out investigations of turbulent heat transfer in pipe flows with the objective of elucidating the effect of the governing parameters, Kármán number (Satake et al., 2000) and Prandtl number (Redjem-Saad et al., 2007) on the turbulent heat transfer quantities. DNS studies were conducted by Satake et al. (2000) at $Re_\tau = 150$, 180, 360, 500 and 1050 for $Pr = 0.71$ while Redjem-Saad et al. (2007) considered fixed value of $Re_\tau = 186$ with $Pr = 0.026$, 0.1, 0.2, 0.4, 0.71 and 1.0. Satake et al. (2000) performed

Table 2
List of computational parameters for previous wall-bounded DNS studies with mixed boundary condition.

Previous DNS	Re_τ	Pr	L/δ	l^+	Δx^+	$\Delta z^+/\Delta r^+$	$\Delta y^+/\Delta(r\theta)^+$
Channel flows							
Kasagi et al. (1992)	150	0.71	5π	2356.2	18.4	[0.08, 4.9]	7.4
Kasagi and Ohtsubo (1993)	150	0.025	5π	2356.2	18.4	[0.08, 4.9]	7.4
Abe et al. (1998)	180	[0.025, 0.1, 0.2, 0.4, 0.71, 5.0]	6.4	1152	9.0	[0.40, 11.5]	4.5
	395	[0.025, 0.2, 0.71]	6.4	2528	9.88	[0.44, 13.0]	4.94
Kawamura et al. (1998b)	180	[0.025, 0.05, 0.1, 0.2, 0.4, 0.6, 0.71, 1.0, 1.5]	6.4	1152	9.0	[0.40, 11.5]	4.5
	180	5.0	6.4	1152	4.5	[0.20, 5.90]	2.25
Kawamoto and Kawamura (1999a)	180	[0.025, 0.71]	6.4	1152	9.0	[0.40, 11.5]	4.5
Kawamura et al. (1999)	180	[0.025, 0.2, 0.71]	6.4	1152	9.0	[0.40, 11.5]	4.5
	395	[0.025, 0.2, 0.71]	6.4	2528	9.88	[0.44, 13.0]	4.94
Kawamura et al. (2000)	180	[0.025, 0.2, 0.71]	6.4	1152	9.0	[0.40, 11.5]	4.5
	180	1.0	6.4	1152	4.5	[0.20, 5.90]	2.25
	395	[0.025, 0.71]	6.4	2528	9.88	[0.44, 13.0]	4.94
	395	[0.2, 1.0]	6.4	2528	9.88	[0.20, 9.46]	4.94
Matsubara et al. (2001)	150	0.71	7.85	1177.5	18.4	[1.03, 9.51]	7.36
Kawamura and Abe (2002)	180	[0.025, 0.71]	12.8	2304	9.0	[0.20, 5.90]	4.5
	395	[0.025, 0.71]	12.8	5056	9.88	[0.15, 6.52]	4.94
	640	[0.025, 0.71]	12.8	8192	8.00	[0.15, 8.02]	4.00
Seki et al. (2003a)	180	0.71	12.8	2304	9.0	[0.20, 5.90]	4.5
	395	0.71	12.8	5056	9.88	[0.15, 6.52]	4.94
Kawamura et al. (2004)	180	[0.025, 0.71]	12.8	2304	9.0	[0.20, 5.90]	4.5
	395	[0.025, 0.71]	12.8	5056	9.88	[0.15, 6.52]	4.94
	640	[0.025, 0.71]	12.8	8192	8.00	[0.15, 8.02]	4.00
	1020	[0.025, 0.71]	12.8	13056	6.38	[0.15, 7.32]	4.25
Tsukahara et al. (2004)	64	0.71	25.6	1638.4	6.40	[0.071, 2.11]	3.20
	70	0.71	25.6	1792	7.00	[0.078, 2.31]	3.50
	80	0.71	51.2	4096	4.00	[0.111, 3.59]	3.52
	80	0.71	12.8	1024	4.00	[0.089, 2.64]	2.00
	110	0.71	12.8	1408	5.50	[0.123, 3.62]	2.75
	150	0.71	12.8	1920	7.50	[0.167, 4.94]	3.75
	180	0.71	12.8	2304	9.00	[0.201, 5.93]	4.50
Seki et al. (2006)	180	[0.71, 1.0, 2.0, 10.0]	6.4	1152	1.1	[0.05, 1.0]	1.1
Antonia et al. (2008)	180	0.71	12.8	2304	3.00	[0.20, 5.90]	3.00
	395	0.71	12.8	5056	3.29	[0.15, 6.52]	3.29
	640	0.71	12.8	8192	4.00	[0.15, 8.02]	4.00
	1020	0.71	12.8	13056	6.38	[0.15, 7.32]	4.25
Kozuka et al. (2009)	180	[0.71, 1.0, 2.0, 10.0]	6.4	1152	1.13	[0.0504, 0.972]	1.13
	180	[7.0, 10.0]	6.4	1152	0.563	[0.0504, 0.972]	1.13
	395	[0.71, 1.0, 2.0, 5.0, 7.0, 10.0]	6.4	2528	1.23	[0.111, 2.13]	2.47
Pipe flows							
Satake et al. (2000)	150	0.71	15	2250	8.78	[0.24, 0.86]	7.36
	180	0.71	15	2700	10.5	[0.29, 1.04]	8.84
	360	0.71	15	5400	14.0	[0.11, 1.1]	8.83
	500	0.71	15	7500	14.6	[0.1, 2.6]	8.18
	1050	0.71	15	15750	15.4	[0.163, 4.16]	8.59
Piller (2005)	180	0.71	12.656	2278	7.03		6.28
Redjem-Saad et al. (2007)	186	0.026	15	2790	20	[0.01, 7]	10
	186	[0.1, 0.2, 0.4, 0.71, 1.0]	15	2790	10	[0.01, 5]	10
Saha et al. (2010)	170	[0.026, 0.1, 0.2, 0.4, 0.71, 1.0]	4π	2148.8	14.3	[0.5, 3.6]	8.4

their simulation inside a pipe of length 15δ, which was the same length used by Redjem-Saad et al. (2007). Satake et al. (2000) did not mention why they chose this length or perform any related analysis to justify this pipe length. Redjem-Saad et al. (2007) in their investigation proved that correlations for both velocity and temperature tend to zero at streamwise separation of half the pipe length, indicating that the length of the pipe was sufficient to capture the largest flow eddies as well as thermal structure. Although their results provide a reference pipe length for DNS studies, some doubt remains if this was sufficient for convergence of all relevant statistical information. Meanwhile, Piller (2005) used a shorter pipe of 12.676δ to compare the effect of different thermal boundary conditions on the mean properties and turbulence statistics up to fourth order, the budget and the wavenumber spectra of the temperature fluctuations. Using the autocorrelation function with streamwise separation for velocity and temperature fluctuation, he proposed that the pipe length adopted was marginally sufficient to capture the largest scale structures of the flow and thermal field, even though the computed correlation functions had finite values at streamwise separation of half a pipe length.

So far, no studies have specifically investigated the effect of computational domain length on turbulent heat transfer in pipe flow. Earlier studies of del Álamo et al. (2004) and Abe et al. (2007) showed the effects of the computational domain size on turbulent channel flow. Later, Chin et al. (2010a,b) made a thorough investigation of the convergence of lower and higher order statistics of the flow field as a function of the length of the computational domain. These studies have added valuable information about saving the computational cost when one performs the DNS at high *Re*. For turbulent heat transfer simulation, the work of Tsukahara et al. (2004) provided very limited information on the effects of computational box size on mean and rms of temperature profile and turbulent Prandtl number at $Re_\tau \approx 80$ and $Pr = 0.71$. Their results suggested that the computational domain size should be large enough to capture large scale structures of the thermal fluctuations for very low Reynolds number. However, they only considered two different computational domains and did not include the convergence of higher-order statistics with the change of Prandtl numbers.

The present study investigates how thermal statistics vary with Prandtl number and domain length used in simulations of turbulent pipe flow. The convergence of purely flow-based statistics with domain length for turbulent pipe flow has already been addressed by Chin et al. (2010a,b) and the present paper aims to extend their findings to include statistical turbulent heat transfer quantities. We have carried out a series of DNS in which different pipe lengths are considered for a range of Prandtl numbers while keeping all other parameters and grid resolution fixed at values similar to those considered by Chin et al. (2010a,b) at $Re_\tau \approx 170$. The subsequent comparison among various computed thermal statistics provides a good understanding of domain length required for the convergence of turbulence statistics involving heat transfer quantities.

2. Mathematical formulation

2.1. Model description

The turbulent heat transfer inside a pipe is simulated using the cylindrical domain shown in Fig. 1. The turbulent flow is fully developed, and the incompressible Newtonian fluid is heated with a uniform heat flux q_w imposed at the pipe wall. The fluid properties are assumed constant and temperature is considered to be a passive scalar. The diameter of the pipe is denoted by $D = 2\delta$, and the length of the computational domain by *L*. The length: diameter ratio has been varied on the basis that previous pipe-flow DNS at $Re_\tau \approx 170$ by Chin et al. (2010a,b). That study established that minimum pipe length required for a converged streamwise mean velocity profile is $2\pi\delta$. A length of at least $8\pi\delta$ is required to ensure a minimum level of correlation associated with large-scale turbulent structure, thus establishing the convergence of higher order statistics. Moreover, the selected range of pipe lengths in the present study covers the range of computational domain lengths for all previous DNS studies for both channel and pipe flows at comparable Reynolds and Prandtl numbers as given in Table 2.

2.2. Governing equations

The system under study is governed by the incompressible Navier–Stokes equations

$$\frac{\partial \boldsymbol{u}}{\partial t} + N(\boldsymbol{u}) = -\nabla P + \nu \nabla^2 \boldsymbol{u} + \boldsymbol{F}, \tag{1}$$

$$\nabla \cdot \boldsymbol{u} = 0, \tag{2}$$

where $P = p/\rho$ is the kinematic pressure, ν is the kinematic viscosity, $N(\boldsymbol{u})$ represents the non-linear advection terms and $\boldsymbol{F}$ is a body force vector. Coordinates *x*, *r*, θ indicates the axial, radial and azimuthal directions respectively in a cylindrical co-ordinate system and the velocity $\boldsymbol{u}$ represents $\boldsymbol{u}(x,r,\theta,t) = (u_x, u_r, u_\theta)(t)$. In the present formulation, $N(\boldsymbol{u})$ is implemented in skew-symmetric form for robustness, i.e.

$$N(\boldsymbol{u}) = 0.5[\boldsymbol{u} \cdot \nabla \boldsymbol{u} + \nabla \cdot \boldsymbol{u}\boldsymbol{u}]. \tag{3}$$

The pressure gradient $-\nabla P$ is split into a mean pressure gradient $-\nabla \bar{P}$ and a fluctuating pressure gradient $-\nabla P'$ such that streamwise periodicity can be employed for the fluctuating pressure P'. The mean pressure gradient $-\nabla P$ only has a non-zero component in the streamwise direction in order to balance the net viscous friction at the pipe wall. For a fully developed turbulent pipe flow the driving force $\boldsymbol{F} = (F,0,0)$ (body force per unit mass) corresponds to the mean pressure gradient in streamwise *x*-direction,

$$F = \frac{4\tau_w}{\rho D}, \tag{4}$$

which allows both the pressure and velocity to be periodic in the streamwise direction. In the present study, the unit length scale is pipe diameter *D*, and the unit velocity scale is U_b, which is defined as the ratio of mean volumetric flow rate and pipe cross-sectional area ($4\langle Q\rangle/\pi D^2$). The time scale is therefore D/U_b. The bulk Reynolds number $Re_D = U_b D/\nu = 5000$ is selected to be the same as the simulations carried out by Chin et al. (2010a,b). Wall shear stress, τ_w, is calculated using the Blasius relationship to allow the body force to be present. The Blasius friction factor correlation for smooth pipes (Blasius, 1913),

$$\lambda = \frac{4\tau_w}{0.5\rho U_b^2} = \frac{0.3164}{Re_D^{1/4}}, \tag{5}$$

is used to estimate the wall shear stress τ_w. The friction velocity $u_\tau = (\tau_w/\rho)^{1/2}$ and the body force required per unit mass to drive the flow is

$$F = \frac{\lambda \rho U_b^2}{2D}. \tag{6}$$

From Eq. (5), the smooth–pipe relationship can be obtained as,

$$Re_\tau = \frac{u_\tau D}{2\nu} = 99.436 \times 10^{-3} Re_D^{7/8}, \tag{7}$$

where $Re_\tau = u_\tau D/2\nu$ is the Kármán number and for $Re_D = 5000$ in the present study, $Re_\tau \approx 170$. The spatial and temporal evolution of the

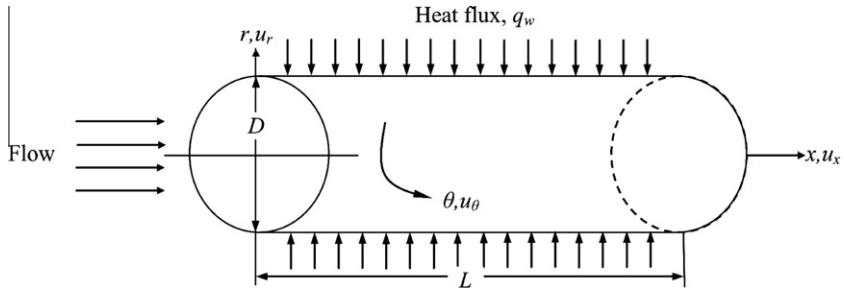

Fig. 1. Schematic of pipe flow configuration.

governing Eq. (1) can be written in dimensionless form, using U_b and D as velocity and length scales for normalization, as

$$\frac{\partial \boldsymbol{u}}{\partial t} + N(\boldsymbol{u}) = -\nabla P + \frac{1}{Re_D}\nabla^2 \boldsymbol{u} + \left(\frac{4Re_\tau}{Re_D}\right)^2. \tag{8}$$

The transport equation for passive scalar (temperature) is governed by the dimensional energy equation for the thermal field in the form of an advection–diffusion problem:

$$\frac{\partial T}{\partial t} + \boldsymbol{u}\cdot\nabla T = \alpha\nabla^2 T, \tag{9}$$

where α is known as thermal diffusivity which can be expressed as

$$\alpha = \frac{k}{\rho c_p} = \frac{\nu}{Pr}. \tag{10}$$

The dimensionless temperature Θ is defined as:

$$\Theta = \frac{\langle T_w\rangle - T}{T_r}, \tag{11}$$

where $T_r = q_w/\rho C_p U_b$ is a reference temperature and $\langle T_w\rangle$ denotes the wall temperature averaged in time and in the circumferential direction. Normalizing using these variables, the thermal energy equation can be written as

$$\frac{\partial \Theta}{\partial t} + \boldsymbol{u}\cdot\nabla\Theta - u_x\frac{1}{T_r}\frac{\partial\langle T_w\rangle}{\partial x} = \frac{1}{Re_D Pr}\nabla^2\Theta. \tag{12}$$

2.3. Boundary conditions

Axial symmetry boundary conditions (internally setting either as zero essential or zero natural depending on the physical variable and the Fourier mode) for velocity components, pressure and temperature are applied along the axis of the computational domain. At the pipe wall no-slip boundary conditions are imposed for all velocity components whereas Neumann boundary conditions are computed for the pressure. Since the flow is assumed to be fully developed, the velocity field is assumed to be homogeneous in the streamwise direction.

The constant heat flux boundary condition over the wall of the pipe is defined by

$$q_w = k\left.\frac{dT}{dr}\right|_{D/2} = \text{const}. \tag{13}$$

The flow is assumed to be statistically homogeneous in the axial direction, with axial periodicity of velocity, pressure and temperature fields. So the axial temperature gradient should be corrected in order to make the rate of change of ensemble-average temperature invariant at any location. The heating condition imposed on the wall implies a linear increase of the bulk temperature $\langle T_b\rangle$ in the streamwise direction. For fully developed flows, the following equalities are satisfied (Redjem-Saad et al., 2007),

$$\frac{\partial\langle T\rangle}{\partial x} = \frac{\partial\langle T_b\rangle}{\partial x} = \frac{\partial\langle T_w\rangle}{\partial x} = \text{const} \tag{14}$$

and using energy balance for the present problem and from Incropera and Dewit (2000), we have

$$\frac{\partial\langle T_w\rangle}{\partial x} = \frac{4q_w}{\rho c_p U_b} = 4T_r. \tag{15}$$

Using Eq. (15), the dimensionless energy Eq. (12) can be written as

$$\frac{\partial\Theta}{\partial t} + \boldsymbol{u}.\nabla\Theta - 4u_x = \frac{1}{Re_D Pr}\nabla^2\Theta. \tag{16}$$

The thermal boundary condition at the wall is

$$\Theta = 0. \tag{17}$$

By using Eq. (16) and applying boundary condition (Eq. (17)), we are effectively able to satisfy both uniform heat flux and linear axial wall temperature variation simultaneously. Piller (2005) refers to this situation as a mixed type boundary condition.

2.4. Numerical methods

We employ the spectral element method which combines the geometric flexibility of finite elements with the high accuracy of spectral methods. Our implementation is a version of the Semtex DNS code which is able to solve time-varying Navier–Stokes problems (with passive scalar transport) in both Cartesian and cylindrical coordinates using Fourier expansion functions for spatially-periodic directions. Parametrically mapped quadrilateral elements having tensor product Gauss–Lobatto–Legendre (GLL) Lagrange interpolants within each element are employed by this code in order to achieve spectral accuracy. Spectral element scheme employs a spatial discretization with Fourier expansions in one homogeneous direction coupled with two-dimensional spectral elements in the remaining two coordinates. As the pipe flow features statistical homogeneity in the axial and azimuthal directions, Fourier expansion can in turn be applied to each direction separately. Here we choose the discretization that employs Fourier expansions in the azimuth direction and spectral elements in the meridional semi-plane. The velocity $\boldsymbol{u}$ (same for pressure and temperature) can be directly projected onto a set of two-dimensional (the equation is 2D in terms of k and θ) complex Fourier modes,

$$\hat{\boldsymbol{u}}_k(x,r,t) = \frac{1}{2\pi}\int_0^{2\pi}\boldsymbol{u}_k(x,r,\theta,t)e^{-ik\theta}d\theta, \tag{18}$$

where k is the azimuthal wavenumber. The time integration employed here is a second-order velocity-correction method described by Karniadakis et al. (1991) and Guermond and Shen (2003). A complete description of the numerical algorithm along with the problem of dealing with the coordinate singularity is given in Blackburn and Sherwin (2004).

Table 3
List of present simulation conditions.

Pr	0.025, 0.71, 2.0
Re_τ	170
L	$\pi\delta$, $2\pi\delta$, $4\pi\delta$, $8\pi\delta$, $12\pi\delta$
N_x	8, 16, 32, 64, 96
N_r	8
N_θ	128
Δx^+	6.7
Δr^+	[0.5, 3.6]
$\Delta\delta\theta^+$	8.4

2.5. Mesh parameters

Table 3 shows the present simulation conditions consists of three cases based on different Prandtl numbers. For each Prandtl number, the pipe lengths are selected from $\pi\delta$ (shortest) to $12\pi\delta$ (longest) similar to the studies carried out by Chin et al. (2010a,b). The spatial discretization consists of two-dimensional spectral mesh elements ($N_r \times N_x$ grids) in $r-x$ plane combined with N_θ planes of data in the azimuthal direction (see Fig. 2). Within each spectral element, 10th order Gauss–Lobatto–Legendre tensor-product shape functions are used. We have kept both Kármán number and grid resolutions fixed in order to ensure that the variation in the data is purely due to Prandtl number and length of the computational domain. Supplementary calculations were carried out to ensure that the spatial and temporal resolutions used in this study are sufficient to resolve all velocity as well as thermal scales for the Prandtl numbers considered here. A list of previous DNS grid resolution parameters is already tabulated in Table 2 for comparison purposes. The near-wall radial spacing is 0.5 which is higher than Redjem-Saad et al. (2007) with $r^+ \approx 0.01$ at $Re_\tau \approx 186$ but is sufficient to capture the smallest scales for the range of Prandtl numbers ($0.025 \leqslant Pr \leqslant 2.0$). The Prandtl numbers, $Pr = 0.025$, 0.71 and 2.0, are chosen for this study because they are relevant to practical problems involving heat exchange in fluids such as liquid mercury ($Pr = 0.025$), air ($Pr = 0.71$) and liquid CO_2 ($Pr = 2.0$). For this range of Pr, using the scaling law

$$\frac{\delta_v}{\delta_t} \approx Pr^n,$$

(see Bejan (2004)) where n is 1/3 for $Pr \geqslant 1$ and 1/2 for $Pr \ll 1$, the ratio of the thickness of the velocity boundary layer, δ_v, to the thermal boundary layer, δ_t, is approximately 0.1581, 0.8921 and 1.259. Since the thickness of the thermal boundary layer for $Pr = 0.71$ and 2.0 is $\sim O(1)$, we would expect results to be similar for these two cases.

Turbulent flow is initiated from the fully developed velocity and pressure distribution obtained from the data of Chin et al. (2010a,b) whereas initial temperature field for turbulent heat transfer calculations is assumed to be the distribution of the product of streamwise velocity component and the Prandtl number due to the analogous nature of mean profile of both temperature and streamwise velocity component. Statistical data was only taken after all the initial transients have convected out of the computational domain and the temperature field has reached a statistically stationary state. The statistics are calculated over at least 300, 150, 100, 50 and 50 turnover times (TU_b/L, where T is the time duration in which the data is collected and computed) for pipe length of $\pi\delta$, $2\pi\delta$, $4\pi\delta$, $8\pi\delta$ and $12\pi\delta$ respectively for the range of Prandtl number considered here.

3. Results and discussions

3.1. Mean temperature profiles

Study of the convergence of the mean velocity profiles with various pipe lengths at low Re_τ has been performed by Chin et al. (2010b) and will not be repeated here. In this paper, we will concentrate on how the statistics of the thermal field are influenced by the axial length of the computational domain. The variation of mean temperature profile with pipe lengths and various Prandtl numbers is shown in Fig. 3. The mean temperature normalized using the friction temperature ($\Theta_\tau = q_w/\rho C_p u_\tau$) as a function of normalized wall distance is shown in Fig. 3a, c and e whereas Fig. 3b, d and f shows the same profile normalized by the mean center-line temperature $\overline{\Theta}_c$ from the pipe center to the wall. Similar to mean velocity profile (not shown here), the lack of convergence for the mean temperature is observed at pipe length of $\pi\delta$ for all three Prandtl numbers. Since (studies by Chin et al. (2010a,b) have shown that) the mean velocity only starts to converge from a pipe length

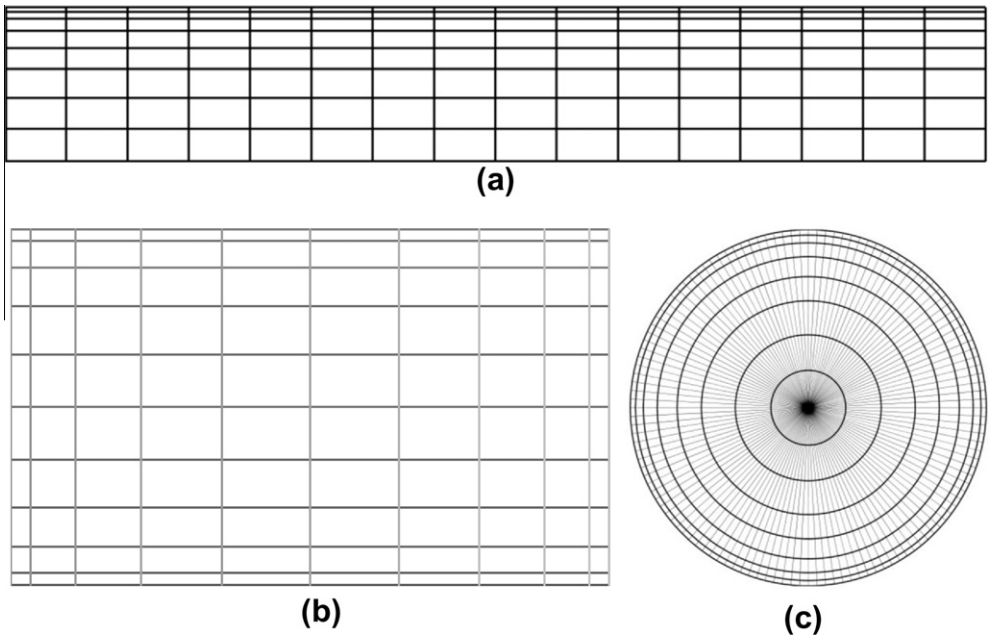

Fig. 2. (a) Two-dimensional section of spectral element mesh for pipe length $L = \pi\delta$, (b) GLL interpolation node distribution along each mesh element and (c) a Fourier expansion with 64 modes used in the azimuthal direction.

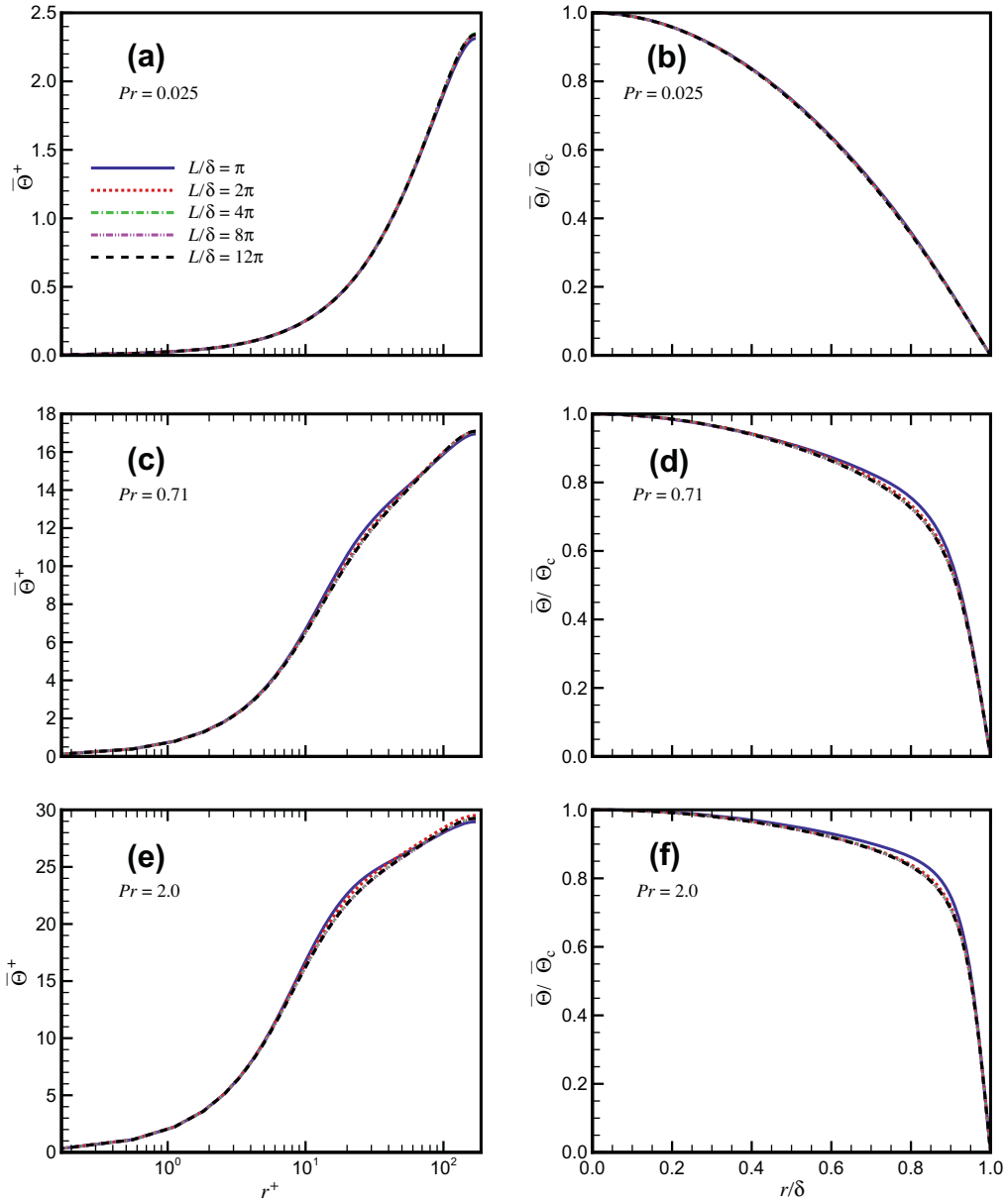

Fig. 3. Mean temperature profile normalized by (a), (c) and (e) the friction temperature Θ_τ and (b), (d) and (f) the center-line temperature $\overline{\Theta}_c$. The lines used are the same for three different Pr to represent pipe lengths: $\pi\delta$ (—), $2\pi\delta$ (···), $4\pi\delta$ (– · –), $8\pi\delta$ (– – · –) and $12\pi\delta$ (––).

of $2\pi\delta$, and the dynamics of the thermal field is dependent on the dynamics of the flow field, it is obvious that the mean temperature field would not show any convergence for any pipe shorter than $2\pi\delta$. There is no remarkable discrepancy of mean temperature exist for $Pr = 0.025$ except at the center of the pipe, but the results for $Pr = 0.71$ and 2.0 clearly show the effect of shorter pipe on mean profiles. For high Prandtl number ($Pr = 2.0$), even pipe length of $2\pi\delta$ is not sufficient to produce converged profile. This is clearly noticeable from the buffer layer to the outer region when the pipe length is measured in wall units (see Fig. 3e), but when scaled with δ the dependence of the domain length near the pipe center is not visible at all. It is clear that the convergence of mean temperature strongly depends on the magnitude of Prandtl number and the results confirm that it is necessary to consider longer pipe for higher Pr. Hence, the minimum length required to have converge mean temperature profile for $Pr = 0.025$ and 0.71 is $2\pi\delta$ (approximately 1000 wall units) and $4\pi\delta$ (approximately 2100 wall units) for other higher Prandtl numbers considered here.

3.2. RMS of fluctuating temperature profiles

According to the convergence study by Chin et al. (2010a,b) for rms values of the streamwise fluctuating velocity, it was proposed that the minimum length was $4\pi\delta$ corresponding to $l^+ = O(2100)$ for $Re_\tau \approx 170$. A similar study is carried out here to determine the minimum domain length required for convergence of statistics related to the fluctuating temperature field for different Prandtl numbers. We have plotted rms profile of the fluctuating temperature normalized by the friction temperature as a function of normalized wall-normal distance in Fig. 4a–c for $Pr = 0.025$, 0.71 and 2.0 respectively. As expected like fluctuating velocity profile (not shown here), the profile $\Theta^{\prime+}_{\mathrm{rms}}$ for $\pi\delta$ varies significantly from the other pipe lengths. Further, these variation is not only limited to the vicinity of the peak rms location but also near the center of the pipe depending on the magnitude of the Prandtl number. The reason for a higher value in the peak turbulence intensity for DNS of shorter pipe flow was described by Chin et al. (2010b). They

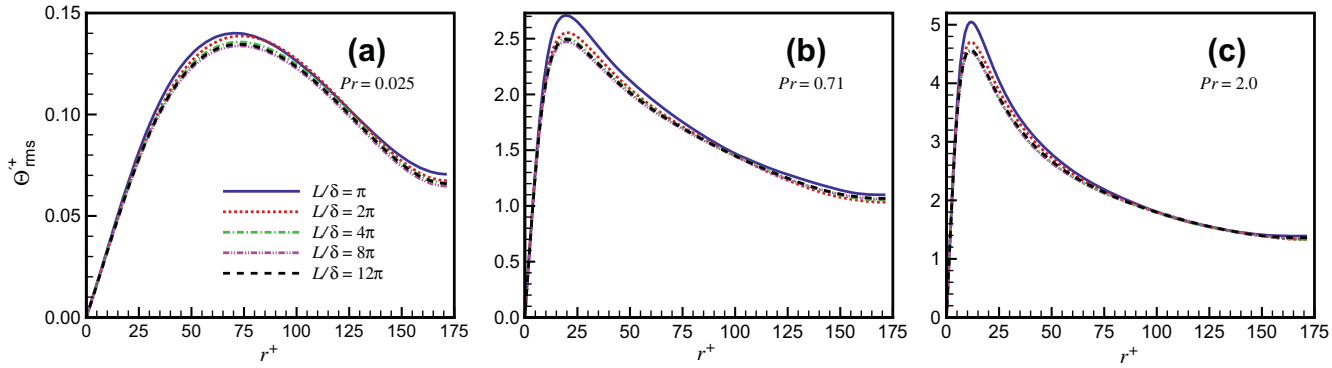

Fig. 4. RMS of temperature fluctuation normalized by the friction temperature Θ_τ for different pipe lengths at (a) $Pr = 0.025$, (b) $Pr = 0.71$ and (c) $Pr = 2.0$. Lines used are as in Fig. 3. Scales shown in y-axis of each figure are given in different ranges.

showed that an artifact of insufficient pipe length was a higher value in the peak turbulence intensity and further investigations of cross-correlation functions confirmed the existence of massive periodic structures at shorter pipe contributing larger peak value. Hence it is consistent here to have a similar higher value of the peak rms temperature fluctuation for simulations carried out with pipe lengths that are too short. Owing to the decrease in thickness of the thermal boundary layer, the location of peak rms value moves closer to the wall as the molecular Prandtl number increases (Redjem-Saad et al., 2007; Saha et al., 2010). At $Pr = 2.0$, even pipe length of $2\pi\delta$ does not give any converged peak rms value. Convergence of the peak rms value is only achieved for pipe length of $4\pi\delta$. It is interesting to note that at the center of the pipe, there is clear convergence of the fluctuating temperature profiles for all domain length computed here. It is speculated that the discrepancy close to the wall is due to the "contamination" of the smaller scales in the thin thermal boundary layer due to the periodic boundaries. The thermal boundary layer is too thin for the dynamics of the smaller scales to influence the motion at the center of the pipe, hence the smaller variation of the statistics at the center of the pipe. But when $Pr \leqslant 0.71$, the non-convergence of statistics due to the artifacts of the pipe length occurs both at the location of peak rms temperature and the center of the pipe. For $Pr = 0.025$, the pipe length of $4\pi\delta$ is sufficient to give converged peak value and at the pipe center, the difference of having enhanced $\Theta'^{+}_{\mathrm{rms}}$ is easily compared from the result for the longest pipe length. The value of the converged peak intensity for $Pr = 0.71$ is 2.48 at a wall-normal location of $r^+ \approx 19.4$. Like $Pr = 0.025$, the minimum length for $Pr = 0.71$ is $4\pi\delta$ which does not seem to differ noticeably from the longer pipe lengths in any other radial location. However, it is clear that with the increase of Prandtl number, there is better convergence of rms profiles near the pipe center for all values of L/δ. This results seem to suggest the presence of structures with smaller length scales at the pipe center at higher Prandtl number. Finally, for all Prandtl numbers considered here, the required length is $4\pi\delta$ corresponding to $l^+ = O(2100)$ which is consistent with the findings of Chin et al. (2010a,b).

3.3. Streamwise two-point correlations

The traditional way to choose a minimum domain length is to investigate two-point correlations of the fluctuating velocity components and temperature (Lyons et al., 1991; Piller, 2005; Redjem-Saad et al., 2007) from where one can also obtain information about the structure of the turbulent flow and thermal field. The methodology used to calculate streamwise two-point correlation of the fluctuating temperature has adopted from Ganapathisubramani et al. (2005). Since periodicity is employed in the streamwise direction, distribution of the two-point correlation coefficients is symmetric for the location corresponding to half of the computational domain, $L/2$. The contours of the two-point autocorrelations of fluctuating temperature are presented as a function of wall-normal location (r^+) and streamwise separation in Fig. 5. The separation distance is non-dimensionalized by the inner variable (u_τ/ν) rather than by the outer variable (δ). Here the outermost correlation contour lines have a value of -0.1 within the range of $\Delta x^+(-1200 \leqslant \Delta x^+ \leqslant 1200)$ and the contour interval is 0.1. It is clearly observed in those figures that the abrupt end of contour lines for pipe lengths $\pi\delta$, $2\pi\delta$ and $4\pi\delta$ shows the inadequacy of periodic domain length. The incomplete contour lines for $\pi\delta$ and $2\pi\delta$ signify that they are unable to accommodate the longest thermal streaky structure within the computational domain. The effect of Prandtl number on the correlations of temperature fluctuations also shows an interesting trend. For $Pr = 0.71$ and 2.0, the correlation curves are almost identical to each other due to very similar length scales $\sim O(1)$ and the outermost contour line ($R_{\Theta\Theta} = 0.0$) for pipe length $4\pi\delta$ fails to form a complete curve at $\Delta x^+ \approx 1050$ in Fig. 5b and c. This suggests the limitation of the computational domain for resolving the largest scales of motion due to the periodicity in the streamwise direction. When $Pr = 0.025$, similar behavior for pipe length $4\pi\delta$ is also observed at $\Delta x^+ \approx 1100$. Moreover, the pattern of the contour lines indicates longer size of the thermal streaky structure which will be graphically presented later in this paper. Fig. 6a–c shows the streamwise two-point correlations of the fluctuating temperature at wall-normal location r^+ for maximum $\Theta'^{+}_{\mathrm{rms}}$ for $Pr = 0.025$, 0.71 and 2.0 respectively. The profile of $R_{\Theta\Theta}$ at $r^+ \approx 72$ (which is far away from $r^+ \approx 15$ for maximum $u^+_{x,\mathrm{rms}}$) shows weak periodicity in the streamwise direction for low $Pr = 0.025$. For this Pr, the two-point correlation coefficients reduce to a value close enough to zero as the pipe length increases and become eventually zero when the pipe length is equal or longer than $2\pi\delta$. But this result at this r^+ location does not provide the exact picture of convergence as the correlation curves in Fig. 5a for pipe length up to $4\pi\delta$ do not seem to complete due to the existence of bigger structure size. Interestingly, correlation curves for fluctuating streamwise velocity component crossed zero for the pipe length of $8\pi\delta$ or above (mentioned in Chin et al. (2010b)) although it was measured at $r^+ \approx 15$ whereas at least $8\pi\delta$ is also required to achieve convergence for this low $Pr = 0.025$. The two-point correlations for the other two Prandtl numbers are further characterized by a longer length scale. It can be seen for $Pr \geqslant 0.71$ that the two-point correlations for streamwise component of velocity and temperature are almost identical (Fig. 4a in Chin et al. (2010b)). The decays of the two-point correlations are not enough in the results of $4\pi\delta$ for $Pr = 0.71$ and 2.0 and it is considered here that the computational domain length $4\pi\delta$ is too short to obtain reliable

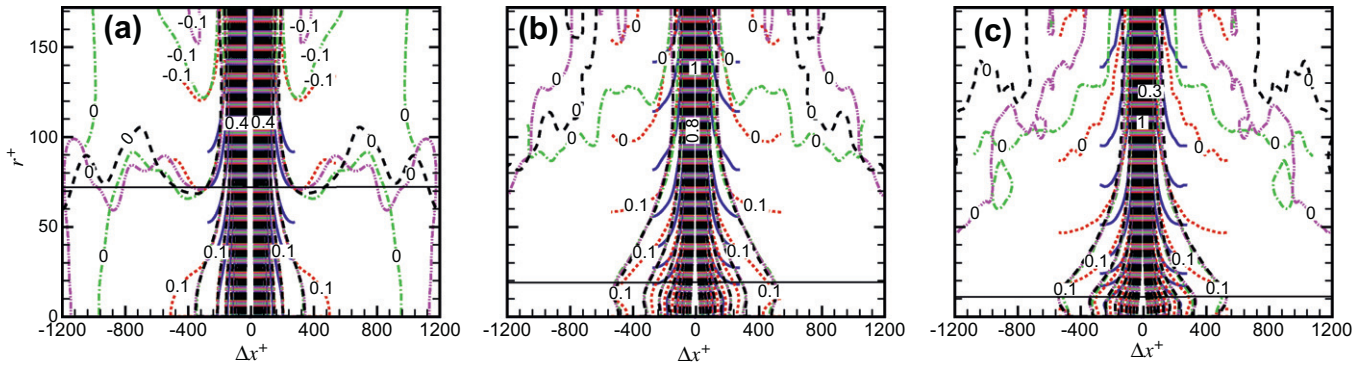

Fig. 5. Contours of autocorrelation coefficient for temperature fluctuations at (a) $Pr = 0.025$, (b) $Pr = 0.71$ and (c) $Pr = 2.0$. Lines used are as in Fig. 3. The solid horizontal line represents the wall-normal location of maximum Θ'^{+}_{rms} at each Pr.

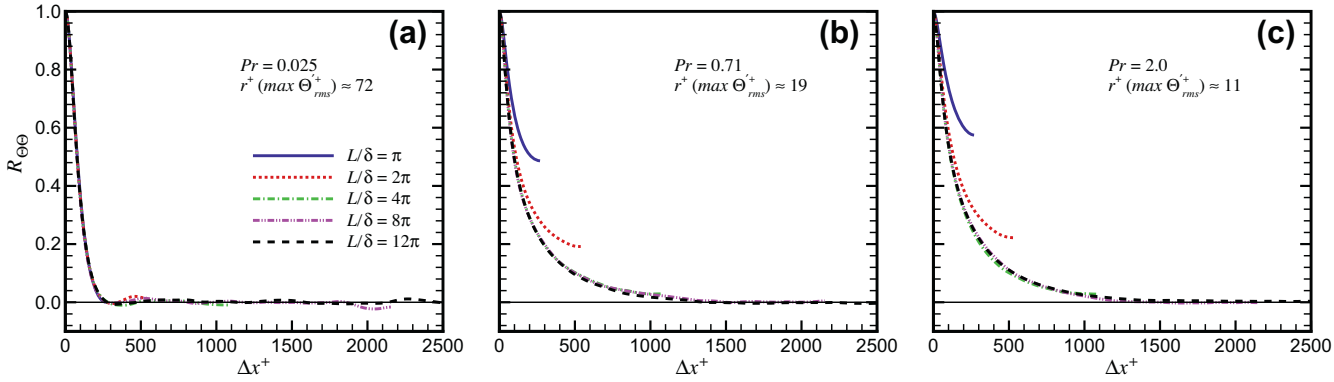

Fig. 6. Streamwise two-point correlation for temperature fluctuation at $r^+ (max\ \Theta'^{+}_{rms})$: (a) $Pr = 0.025$, (b) $Pr = 0.71$ and (c) $Pr = 2.0$. Lines used are as in Fig. 3.

data. When Pr is 2.0, the self-correlation $R_{\Theta\Theta}$ at $8\pi\delta$ falls off more rapidly than $12\pi\delta$ and zero correlations are obtained at a separation less than half the length of the computational domain. This reveals that this pipe length ($8\pi\delta$) is sufficiently adequate to capture the largest scale structure of the thermal field. Besides, the profiles of $R_{\Theta\Theta}$ at $4\pi\delta$ and $8\pi\delta$ for $Pr = 0.71$ are consistent with the results of Redjem-Saad et al. (2007) at $Re_\tau \approx 186$ where they found zero-correlation for the computational length, $L = 15\delta$. For $Pr = 0.71$, the profiles of $R_{\Theta\Theta}$ at $8\pi\delta$ and $12\pi\delta$ closely agree with each other at this r^+ location and they have long tails along $R_{\Theta\Theta} = 0$ over a streamwise distance $\Delta x^+ \approx 1200$, suggesting that the thermal streaky structure of the temperature fluctuation prevails with the long correlation length in the streamwise direction. The effects of various length scales on the convergence of $R_{\Theta\Theta}$ are clearly demonstrated by plotting correlation curves as shown in Fig. 7 at another wall-normal location nearer to the pipe center $r/\delta \approx 0.1$. The smallest thermal length scale due to low Pr (= 0.025) requires the computational length of $8\pi\delta$ to obtain the convergence and the $R_{\Theta\Theta}$ curves cross zero at $x/\delta \approx 1.2$. Although for higher Prandtl numbers ($Pr \geqslant 0.71$) the converged pipe lengths ($L \geqslant 8\pi\delta$) start to cross zero at $x/\delta \geqslant 2.0$, the nature of these curves suggest that even a shorter pipe length would be able to maintain convergence when the thermal length scales grow larger $\gg O(1)$. So the overall results from Fig. 6b and c indicate that convergence is achieved at a pipe length of $8\pi\delta$ corresponding to $l^+ \approx O(4300)$ for $Pr = 0.71$ and 2.0 and the same length is also required for $Pr = 0.025$ as observed in Figs. 5a and 7a.

3.4. Skewness and flatness factors

Higher order statistics such as skewness and flatness (also known as kurtosis) indicate the intermittent characteristics of the wall region. Fig. 8a, c and e represents the radial distributions of skewness coefficient in the near wall region for $Pr = 0.025$, 0.71 and 2.0 respectively. For $Pr = 0.025$, the skewness decays linearly from the wall and the results follow the same trend for pipe length of $2\pi\delta$ to $12\pi\delta$. It is interesting to note that the converged skewness factor for streamwise fluctuating velocity is achieved at a longer pipe length of $4\pi\delta$ (Chin et al., 2010a). When $Pr \geqslant 0.71$, the skewness of the temperature fluctuations at the wall is about 1.0 and it decays rapidly from the wall below the Gaussian value ($S(\Theta') = 0$). The asymmetric fluctuation of temperature in the near wall region is indicated by the non-zero wall value of $S(\Theta')$ which confirms the intermittent behavior close to the wall, however the turbulence is almost homogeneous far from the wall. The value of $S(\Theta')$ for the pipe length of $\pi\delta$ always follows a different trend for all value of Pr due to lack of convergence. On the other hand, pipe length of $2\pi\delta$ for $Pr \geqslant 0.71$ does not show any convergence inside the core region of the pipe although the near-wall behavior is reasonably close to the converged skewness profile. Hence, the minimum length is $2\pi\delta$ for $Pr = 0.025$ and $4\pi\delta$ for other two Prandtl numbers in order to achieve the convergence of third order statistics.

The flatness for fluctuating temperature Θ' in the near wall region is shown in Fig. 8b, d and f for $Pr = 0.025$, 0.71 and 2.0 respectively. It is obvious at $Pr = 0.025$ that results do not converge for pipe length less than $2\pi\delta$. But a closer look of these profiles demonstrates that $8\pi\delta$ and $12\pi\delta$ provide converged flatness factor near the wall. Similar to skewness profiles, for $Pr \geqslant 0.71$, the profiles of the flatness coefficient continuously dominate more near the wall. However, the results for $Pr \geqslant 0.71$ seem to show convergence in the near wall until the pipe length becomes $4\pi\delta$ which is consistent with the converged profile of $F(u'_x)$ as investigated by Chin et al. (2010a). The value of $F(\Theta')$ is also higher near the wall with increase of Pr, indicating more intermittent region. For $Pr \geqslant 0.71$,

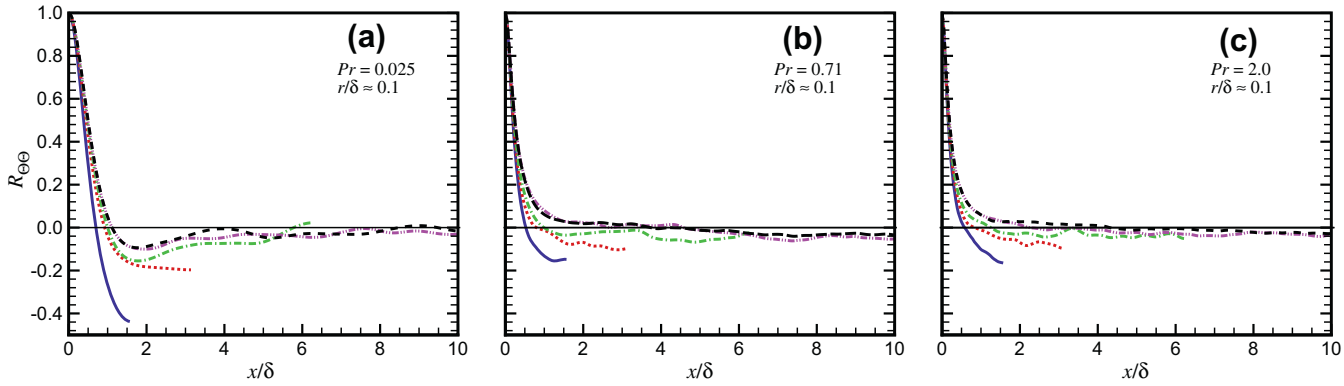

Fig. 7. Streamwise two-point correlation for temperature fluctuation at $r/\delta \approx 0.1$: (a) $Pr = 0.025$, (b) $Pr = 0.71$ and (c) $Pr = 2.0$. Lines used are as in Fig. 3.

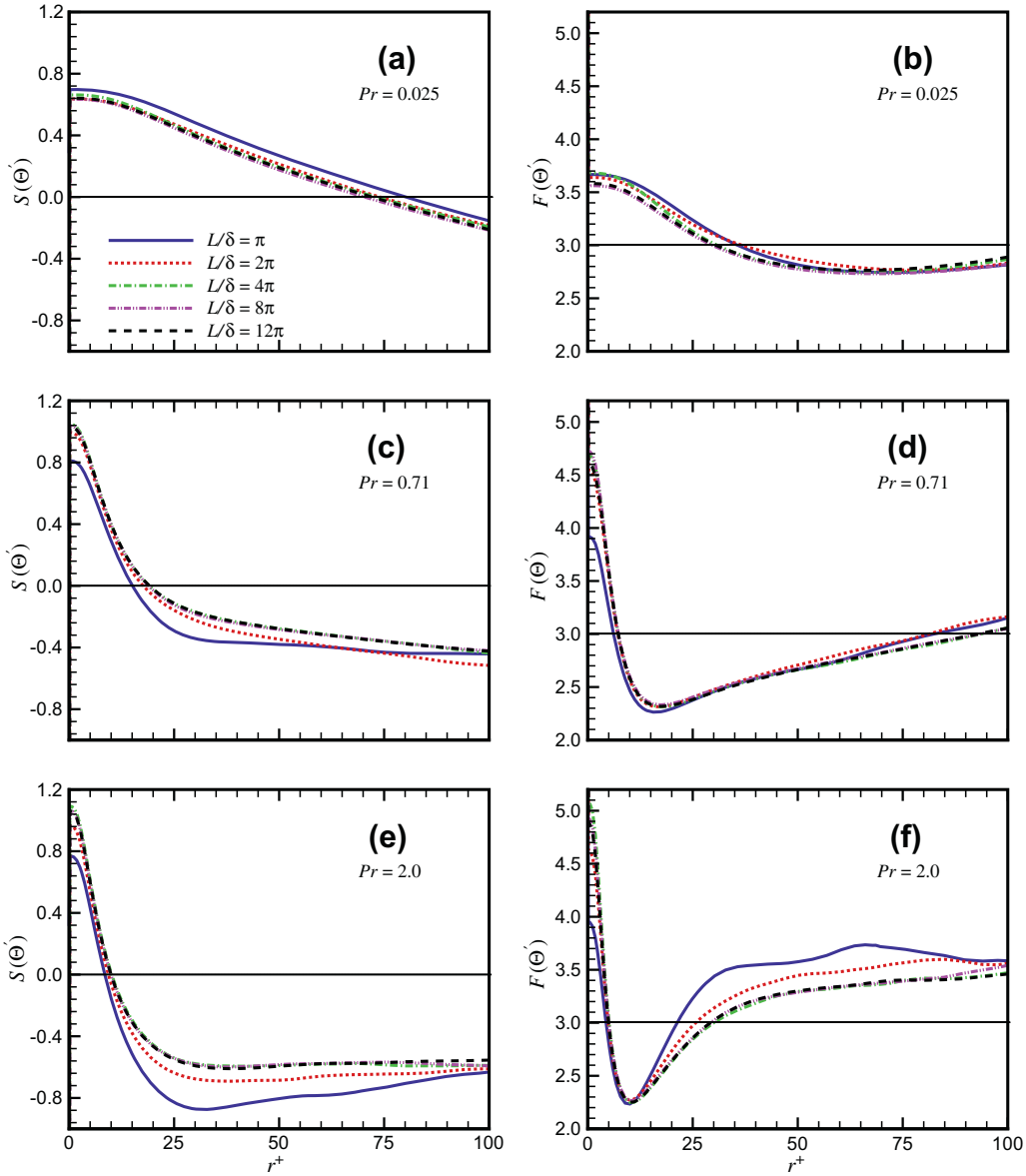

Fig. 8. (a), (c) and (e) Skewness factors and (b), (d) and (f) Flatness factors of the fluctuating temperature for $Pr = 0.025$, 0.71 and 2.0 respectively. Lines used are as in Fig. 3.

the converged value of $F(\Theta')$ at the wall increases slowly from 4.6 to as high as 4.8 at $Pr = 2.0$ showing the probability of observing large variations from the mean temperature in the vicinity of the wall is much higher than in the center of the pipe. However, the wall value for pipe length of $4\pi\delta$ is always higher than the converged $F(\Theta')$ both at $Pr = 0.71$ and 2.0. Far from the wall, the values of the flatness factors tend approximately to the Gaussian values ($F(\Theta') = 3$) for $Pr \leqslant 0.71$, while $F(\Theta')$ for $Pr = 2.0$ deviates from the

Gaussian behavior which confirms similar predictions obtained by Redjem-Saad et al. (2007). Although following the same trend of the converged $S(\Theta')$ and $F(\Theta')$ profiles, there is a definite discrepancy observed in the profiles of $8\pi\delta$ for $Pr = 2.0$. The analogous results of convergence of skewness and flatness factors for both $Pr = 0.71$ and 2.0 also refer to the behavior of similar length scales as mentioned in Section 2.5.

3.5. Turbulent heat fluxes

The turbulent heat flux arises in combination with the temperature and velocity fields. Thus it is also important to realize the convergence nature of velocity fields which in turns affects the convergence of turbulent heat fluxes. Fig. 9a, c and e shows the distribution of streamwise or axial turbulent heat flux normalized by the friction velocity and temperature for three different Prandtl numbers. The nature of the streamwise heat flux is analogous to the rms profile of fluctuating temperature for each Prandtl number. Comparing these figures, it is clear that the peak of the turbulent heat flux increases with the increase of Pr and moves towards the wall as the conductive sublayer becomes thinner. Moreover, the location of the maximum heat flux is found between the maximum of rms streamwise velocity fluctuations and the maximum of rms temperature fluctuation. Since both the streamwise velocity component and the temperature profile are strongly influenced by the pipe length, streamwise heat flux is also affected by the combined effect of these two components. Similar to rms profiles of both streamwise velocity and temperature, it is found that convergence of turbulent heat flux can be achieved for all Pr for pipe length of $4\pi\delta$. However, a marginal difference in the peak value at $Pr = 0.025$ and 0.71 is observed even for longer pipe length of $8\pi\delta$. Furthermore, due to similar length scales, the profiles for both $Pr = 0.71$ and 2.0 show identical trends (see Fig. 9c and e), although higher Prandtl number always ensures convergence with shorter pipe lengths near the center of the pipe. Since both the streamwise fluctuating velocity and the fluctuating temperature for all Pr require a pipe length of $4\pi\delta$ to converge, streamwise heat flux which is their combined effect must require a pipe length of at least $4\pi\delta$ for convergence.

The normalized wall-normal or radial turbulent heat flux is shown in Fig. 9b, d and f. It is noted that strong decrease of radial heat flux is observed at low Prandtl number. This is because the friction temperature (or q_w) used to make $\overline{u_r'\Theta'}$ dimensionless increases with the decrease of Pr. When $Pr \geqslant 0.71$, the wall-normal heat flux is considerably smaller than the streamwise one over the pipe cross-section. Their difference, however, decreases as Pr is decreased and the anisotropy of turbulent heat fluxes is weakened. Furthermore, when the Prandtl number is small, the maximum value of the wall-normal heat flux is observed farther away from the wall than the maximum streamwise heat flux, as the fluctuating radial velocity is damped strongly by the wall. The dependence of the peak value on the pipe length is almost negligible for $Pr = 0.71$ but is still appreciable for $Pr = 0.025$ and 2.0. It is interesting to note that in the central region of the pipe, the radial heat flux does not depend on the pipe length as observed in the case of streamwise heat flux for $Pr = 0.025$. Since the radial velocity component is less affected by the pipe lengths than the streamwise one, the convergence of wall normal heat flux is achieved with shorter pipe length. Moreover, the fluctuating radial velocity has the tendency to decrease with the increase of domain length (Abe et al., 2007) and thus lowers the peak value of the wall-normal heat flux at $L = \pi\delta$ comparing with other pipe lengths from $Pr = 0.025$ to $Pr = 2.0$. Due to this opposite behavior in comparison of the fluctuating temperature, the difference of the peak value in the radial heat flux profiles at $Pr = 0.71$ is considerably small for all pipe lengths. Hence, a pipe length of $4\pi\delta$ for $Pr = 0.025$, $\pi\delta$ for $Pr = 0.71$ and $2\pi\delta$ for $Pr = 2.0$ is sufficient for the statistics to converge, although the longer pipe of $8\pi\delta$ for $Pr = 0.71$ is showing some marginal discrepancy at the peak value. The convergence tendency for this type of statistics is common because Chin et al. (2010a) also obtained converged Reynolds stress for a pipe length of $2\pi\delta$, shorter than the length required for the convergence of the streamwise fluctuating velocity profile.

3.6. Cross-correlations

The correlation coefficients $R_{u_x\Theta}$ for different Prandtl numbers are presented in Fig. 10. For $Pr \leqslant 0.71$, pipe length of at least $2\pi\delta$ leads to very identical results for these coefficients, except for $r^+ > 125$. In the inner layer for all Pr, the coefficients for $L \geqslant 2\pi\delta$ are almost coincident, while the coefficients for $L = \pi\delta$ always predict higher value, since the flow configuration has a weak effect, resulting in slightly larger correlation coefficients for shorter pipes. The cross-correlation coefficient of the streamwise turbulent heat flux for $Pr \geqslant 0.71$ is larger than that for $Pr = 0.025$, throughout the pipe section. These results mean that the temperature fluctuations are better correlated with streamwise velocity fluctuations for higher Prandtl numbers. When $Pr = 0.025$ and 0.71, the value of $R_{u_x\Theta}$ near the wall is almost similar for any pipe length longer than $\pi\delta$, but a closer observation indicates that the coefficient for pipe length of $4\pi\delta$ tends to deviate from the converged value for $r^+ > 125$. On the other hand, due to analogous profile of streamwise velocity and temperature fluctuation at higher Pr, the correlation curves begin to show reasonable convergence for any pipe length above $2\pi\delta$. The minimum lengths therefore required to get the converged cross-correlation coefficients are $8\pi\delta$ for $Pr \leqslant 0.71$ and $4\pi\delta$ for $Pr = 2.0$.

The effect of streamwise periodicity can also be studied by using two dimensional contour plots of cross-correlation function. We have drawn the cross-correlation coefficients between radial velocity component and temperature fluctuation in Fig. 11. The contours of $R_{u_r\Theta}$ are plotted as a function of r^+ and normalized streamwise separation distance (Δx^+) for different pipe lengths. Inside the outer layer, there are no significant differences in the radial correlation coefficients, but the different distributions of the radial turbulent heat flux near the wall are mainly due to the different intensity of the temperature fluctuations. Although the temperature fluctuations in the inner layer are strongly damped due to the presence of the isothermal ($\Theta = 0$) wall type boundary condition, the temperature field is characterized by lower wavenumber velocity fluctuations leading to smaller $R_{u_r\Theta}$ (Piller et al., 2002). The results for shorter pipe length ($\pi\delta$) are omitted in these contour plot as it has the tendency to show lack of convergence for most of the thermal statistics computed in the previous sections. Besides, even a slightly longer pipe length ($2\pi\delta$) as shown in Fig. 11 fails to accommodate the longest structures in the thermal field. This is clearly evident when the contour lines ($R_{u_r\Theta} = 0.02$) for $L = 2\pi\delta$ do not close, resulting in "contamination" of structure in the thermal field (in an average sense) due to the periodicity in the streamwise direction. When $Pr \geqslant 0.71$, insufficient pipe length like $2\pi\delta$ always clearly shows incomplete structure through the value of $R_{u_r\Theta}$ at 0.05. This would definitely suggest that only pipe length of $4\pi\delta$ enables us to provide complete thermal structure for all Prandtl numbers.

3.7. Instantaneous thermal fields

Finally, the instantaneous temperature fields are visualized to explore how the near wall structures are affected by the Prandtl numbers. The volume visualized has the half-cut view of pipe of having length, $L = 8\pi\delta$ as shown in Fig. 12a–c for $Pr = 0.025$, 0.71 and 2.0 respectively. Here the instantaneous temperature

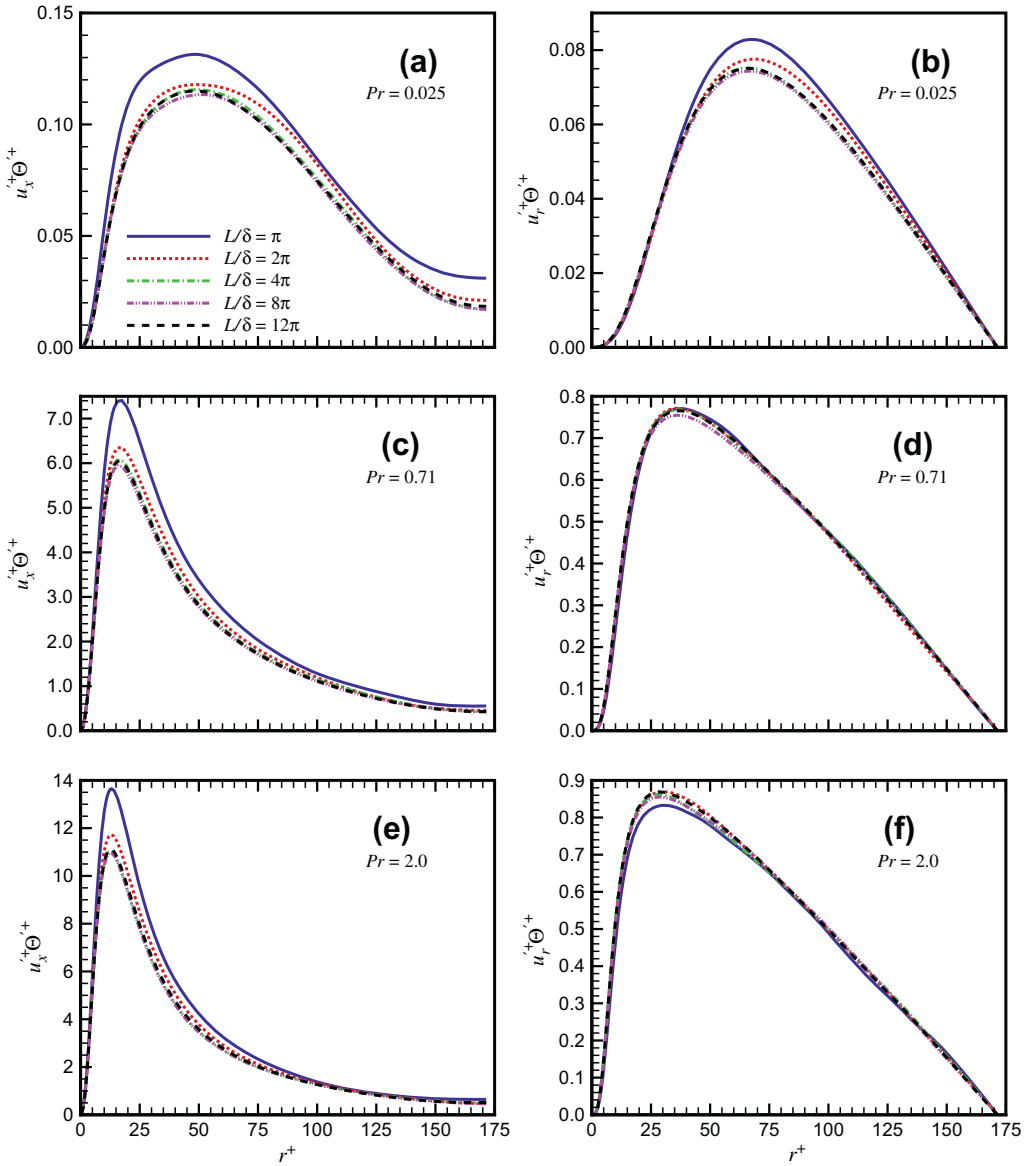

Fig. 9. (a), (c) and (e) Streamwise turbulent heat flux and (b), (d) and (f) Radial turbulent heat flux normalized by the friction velocity u_τ and temperature Θ_τ. Lines used are as in Fig. 3.

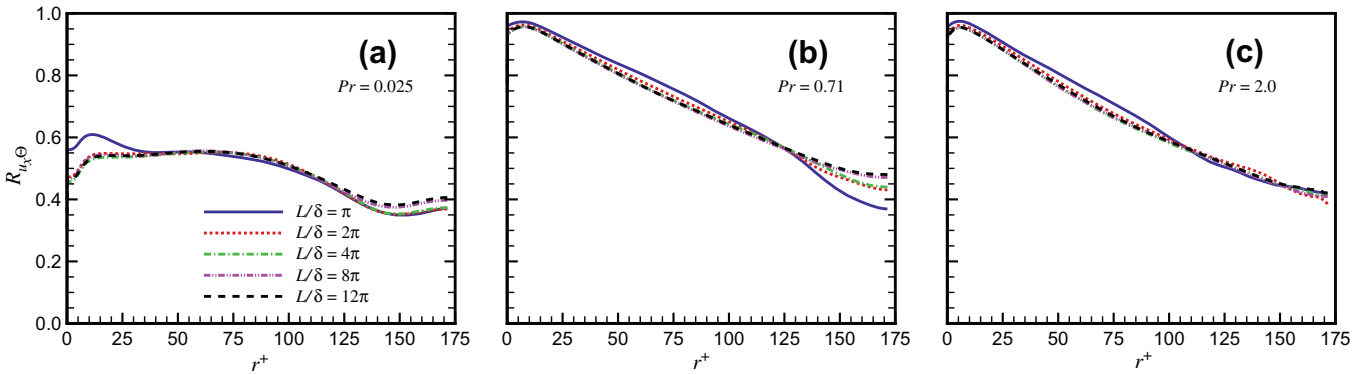

Fig. 10. Cross-correlation coefficient between streamwise velocity component and temperature fluctuations for (a) $Pr = 0.025$, (b) $Pr = 0.71$ and (c) $Pr = 2.0$. Lines used are as in Fig. 3.

fluctuations for each Pr are normalized by their own rms values at each r^+ in order to evaluate the outer-layer structure adequately. Note that the fluid flows from the bottom left to the top right and the contour surfaces of high (white) and low (black) temperature regions are only visualized. The high and low temperature regions imply $+\Theta'/\Theta'_{\mathrm{rms}}$ and $-\Theta'/\Theta'_{\mathrm{rms}}$ where Θ' represents the

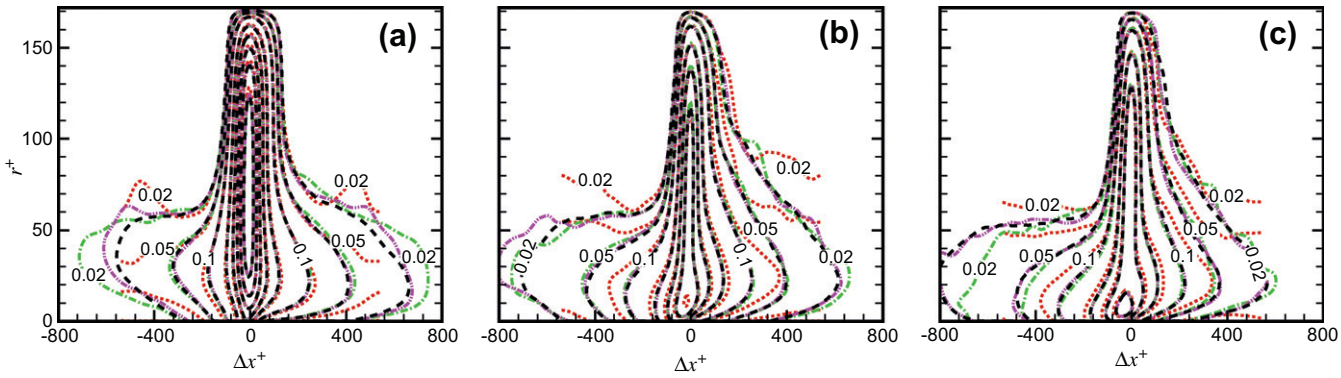

Fig. 11. Contours of cross-correlation coefficient between radial velocity component and temperature fluctuations for (a) $Pr = 0.025$, (b) $Pr = 0.71$ and (c) $Pr = 2.0$. Lines used are as in Fig. 3.

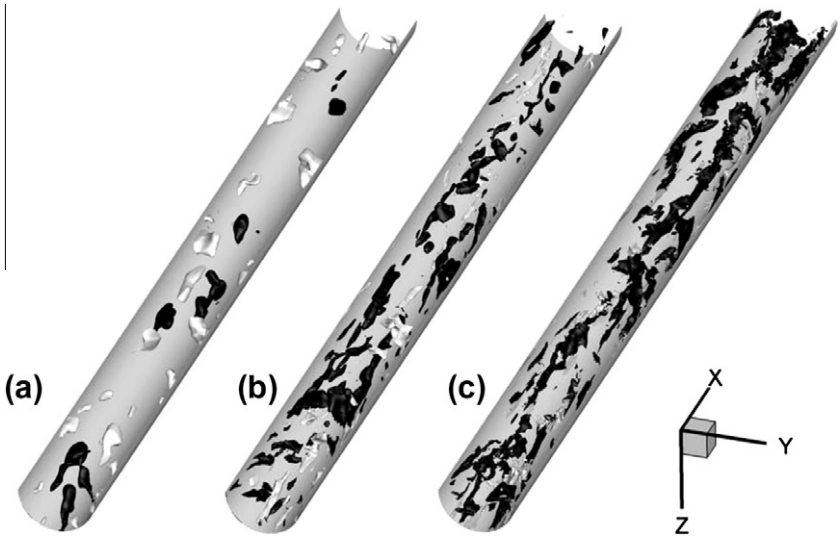

Fig. 12. Iso-surfaces of large-scale structures of the instantaneous temperature fluctuations normalized by their own rms value at each r^+ for $L/\delta = 8\pi$; (a) $Pr = 0.025$, (b) $Pr = 0.71$ and (c) $Pr = 2.0$ (White, $\Theta'/\Theta'_{rms} = 2.0$ and black, $\Theta'/\Theta'_{rms} = -2.0$). The direction of the flow is from bottom-left to top-right.

fluctuating part of the temperature. Thermal streaky structures are observed more frequently and are of small size for $Pr \geqslant 0.71$, while at $Pr = 0.025$, they show several typical 'fatter' shaped structures. This feature has already been observed by Abe et al. (2004) and Kawamura et al. (2004) in their study of thermal structure in a turbulent channel flow. Moreover, there are no sharp temperature gradients along the upstream edge of the large-scale structures which are referred to as "temperature front" by Chen and Blackwelder (1978) in a turbulent thermal boundary layer flow. The difference between the positive and negative temperature fluctuating regions near the wall for $Pr = 0.025$ reflects in the $R_{\Theta\Theta}$ profile inside the inner layer reported in Fig. 5a.

In case of a low Prandtl number of $Pr = 0.025$, the thermal streaks are not elongated in the streamwise direction and their radial spacing seems to be larger compared with that of $Pr \geqslant 0.71$. The conduction layer becomes thicker leading to a reduction of the turbulent heat flux (see Fig. 9a and b) and these trends are more pronounced for lower Prandtl numbers. With the increase of the Prandtl number, the structure of temperature fluctuation is seen to become elongated in the streamwise direction and more slender in the radial direction because the viscous effect becomes less dominant in the thermal field. Moreover, the high and low temperature regions are confined closer to the wall. For $Pr = 0.025$, on the other hand, those regions exist away from the wall and extend up to the central region and takes the complicated lumped shape due to these strong thermal diffusion. This tendency agrees well with the profiles of the temperature variance, which exhibits the peak position at $r^+ \approx 72$ (see Fig. 4a). Besides, this is in accordance with the low correlation coefficient $R_{u_x\Theta}$ in the wall vicinity found in Fig. 10a. A comparison of Fig. 12b and c indicated that positive and negative large-scale structures for $Pr = 0.71$ show a strong similarity to those for $Pr = 2.0$ and they do not appear at approximately same locations, although the shape of these

Table 4
List for required computational pipe length for convergence of various thermal turbulence statistics at $Re_\tau \approx 170$ for three different Prandtl numbers. The minimum lengths are expressed in terms of pipe radius (δ) and within the brackets (), it is given in terms of viscous wall unit (l^+).

Thermal statistics	Min length, $\delta(l^+)$		
	$Pr = 0.025$	$Pr = 0.71$	$Pr = 2.0$
Mean temperature profile	$2\pi(1000)$	$2\pi(1000)$	$4\pi(2100)$
RMS temperature profile	$4\pi(2100)$	$4\pi(2100)$	$4\pi(2100)$
Two-point correlation	$8\pi(4300)$	$8\pi(4300)$	$8\pi(4300)$
Skewness, $r^+ < 100$	$2\pi(1000)$	$4\pi(2100)$	$4\pi(2100)$
Flatness, $r^+ < 100$	$8\pi(4300)$	$4\pi(2100)$	$4\pi(2100)$
Streamwise heat flux	$4\pi(2100)$	$4\pi(2100)$	$4\pi(2100)$
Radial heat flux	$4\pi(2100)$	$\pi(500)$	$2\pi(1000)$
Cross-correlation (streamwise heat flux)	$8\pi(4300)$	$8\pi(4300)$	$4\pi(2100)$
Cross-correlation (radial heat flux)	$4\pi(2100)$	$4\pi(2100)$	$4\pi(2100)$

structures for $Pr = 2.0$ becomes more obscure than those of the structures for $Pr = 0.71$ due to the enhanced convective effect.

4. Conclusions

Effects of various computational pipe lengths on lower and higher order thermal statistics have been comprehensively investigated in the present study. Turbulent statistics of the velocity and thermal field were computed for five different pipe lengths ($\pi\delta$ to $12\pi\delta$) at three different Prandtl numbers (0.025, 0.71 and 2.0). It is found that convergence of statistical information is largely dependent on the type of statistics and Prandtl number. Due to the similarity in the thermal length scales, the convergence of thermal statistics is very similar for $Pr = 0.71$ and 2.0. In general, the thermal length scales for $Pr = 0.025$ is longer than for $Pr = 0.71$ and 2.0, hence it is more difficult to obtain convergence for lower $Pr = 0.025$. This data is summarized in Table 4.

It is clear from Table 4 that using a pipe length that is too short will result in the convergence of the lower order statistics only. In contrast, computing the solution with a longer pipe length than is required will make the simulation costly and time consuming. Our data shows that there is no convergence for any statistics for simulations carried out at the shortest pipe length of $\pi\delta$. Even when the pipe length is $2\pi\delta$, convergence of the mean temperature profile can only be obtained at low Pr. On the other hand, a pipe length of $8\pi\delta$ or longer is only required if one needs to compute converged statistics for two-point autocorrelation and streamwise cross-correlation. Most of the higher order statistics for $Pr = 0.71$ tend to converge with computations carried out with pipe length of $4\pi\delta$. In order to obtain converged statistics for the radial heat flux, which is mainly dependent on the convergence of statistics for the fluctuating radial velocity as described in Section 3.5, the choice of pipe length is quite sensitive to variations in the Prandtl number. Our results show that convergence of the radial heat flux profile can occur even for pipe length as short as $\pi\delta$. In order to explain this anomaly, we need to look at the profiles of the fluctuating radial velocity (see Fig. 1 in Abe et al. (2007)) and temperature (see Fig. 4). It is clear from these figures that close to the pipe wall, magnitude of the fluctuating radial velocity increases with decreasing pipe length (similar results can be found in Abe et al. (2007)). On the other hand, profiles of temperature fluctuations show the opposite trend (i.e. magnitude of the fluctuating temperature decreases with increasing pipe length). Since the radial heat flux is computed from temperature and radial velocity fluctuations, these two opposing effects seem to make the profiles of radial heat flux less sensitive to variations in the pipe length and give the perception this statistic converges with a short domain length $L = \pi\delta$ for $Pr = 0.71$ (see Fig. 9d).

The convergence of most statistical quantities can be achieved if the computations were carried out with a pipe length of $4\pi\delta$ for $0.025 \leqslant Pr \leqslant 2.0$. However, to ensure the convergence of all statistical information for the range of Pr mentioned above, data in Table 4 shows that simulations need to be carried out with a pipe length of $8\pi\delta$. The present findings also point out an important shortcoming of recent DNS simulations carried out for turbulent heat transfer in channel flow. From the results in this paper, it is very likely that some of recent statistical profiles published in the open literature may not be correct as the domain size used in the calculations might not be big enough for some of the statistics to converge.

Acknowledgements

This research was supported by a Victorian Life Sciences Computation Initiative (VLSCI) grant on its Peak Computing Facility at the University of Melbourne, an initiative of the Victorian Government. We would also like to gratefully acknowledge Victorian Partnership for Advanced Computing (VPAC) for initially providing computational resources.

References

Abe, H., Antonia, R., Kawamura, H., 2008. Transport equations for the enstrophy and scalar dissipation rate in a turbulent channel flow. In: 7th International Symposium on Engineering Turbulence Modelling and Mesurements, vol. 3. Limassol, Cyprus, pp. 750–755 (4–6 June).

Abe, H., Kawamura, H., 2002. A study of turbulence thermal structure in a channel flow through DNS up to $Re_\tau = 640$ with $Pr = 0.025$ and 0.71. In: 9th European Turbulence Conference, pp. 399–402.

Abe, H., Kawamura, H., Matsuo, Y., 1998. DNS of turbulent heat transfer in channel flow: near-wall turbulence quantities. In: 13th Australasian Fluid Mechanics Conference. Melbourne, Australia, pp. 849–852 (13–18 December).

Abe, H., Kawamura, H., Matsuo, Y., 2004. Surface heat-flux fluctuations in a turbulent channel flow up to $Re_\tau = 1020$ with $Pr = 0.025$ and 0.71. International Journal of Heat and Fluid Flow 25 (3), 404–419.

Abe, H., Kawamura, H., Toh, S., Itano, T., 2007. Effects of the Streamwise Computational Domain Size on DNS of a Turbulent Channel Flow at High Reynolds Number, vol. 117. Springer-Verlag, Berlin Heidelberg, pp. 233–235.

Antonia, R., Abe, H., Kawamura, H., 2008. Spectral analogy between velocity and scalar fields in a turbulent channel flow. In: 7th International Symposium on Engineering Turbulence Modelling and Mesurements, vol. 1. Limassol, Cyprus, pp. 181–186 (4–6 June).

Bejan, A., 2004. Convection Heat Transfer, third ed. John Wiley and Sons, Inc.

Blackburn, H., Sherwin, S., 2004. Formulation of a Galerkin spectral element Fourier method for three-dimensional incompressible flows in cylindrical geometries. Journal of Computational Physics 197 (2), 759–778.

Blasius, H., 1913. Das ahnlichkeitsgesetz bei reibungsvorgangen in flussigkeiten. Mitteilungen über Forschungsarbeiten auf dem Gebiete des Ingenieurwesens 131, 1–41.

Chen, C.-H.P., Blackwelder, R.F., 1978. Large-scale motion in a turbulent boundary layer: a study using temperature contamination. Journal of Fluid Mechanics 89 (01), 1–31.

Chin, C., Ooi, A., Marusic, I., Blackburn, H., 2010a. The influence of pipe length in direct numerical simulation. In: 17th Australasian Fluid Mechanics Conference. Auckland, New Zealand (5–9 December).

Chin, C., Ooi, A., Marusic, I., Blackburn, H., 2010b. The influence of pipe length on turbulence statistics computed from direct numerical simulation data. Physics of Fluids 22, 115107.

del Álamo, J.C., Jiménez, J., Zandonade, P., Moser, R.D., 2004. Scaling of the energy spectra of turbulent channels. Journal of Fluid Mechanics 500, 135–144.

Ganapathisubramani, B., Hutchins, N., Hambleton, W.T., Longmire, E.K., Marusic, I., 2005. Investigation of large-scale coherence in a turbulent boundary layer using two-point correlations. Journal of Fluid Mechanics 524 (1), 57–80.

Guermond, J., Shen, J., 2003. Velocity-correction projection methods for incompressible flows. SIAM Journal on Numerical Analysis 41 (1), 112–134.

Incropera, F., Dewit, D., 2000. Fundamentals of Heat and Mass transfer, fourth ed. John Wiley and Sons.

Jiménez, J., 2003. Computing high-Reynolds-number turbulence: will simulations ever replace experiments? Journal of Turbulence 4, N22.

Johansson, A., Wikström, P.M., 1999. DNS and modelling of passive scalar transport in turbulent channel flow with a focus on scalar dissipation rate modelling. Flow, Turbulence and Combustion 63, 223–245.

Karniadakis, G., Israeli, M., Orszag, S., 1991. High-order splitting methods for the incompressible Navier–Stokes equations. Journal of Computational Physics 97 (2), 414–443.

Kasagi, N., Iida, O., 1999. Progress in direct numerical simulation of turbulent heat transfer. In: 5th ASME/JSME Joint Thermal Engineering Conference. San Diego, California, pp. 1–17 (March 15–19).

Kasagi, N., Ohtsubo, Y., 1993. Direct Numerical Simulation of Low Prandtl Number Thermal Field in a Turbulent Channel Flow, vol. 8. Springer, Berlin, pp. 97–119.

Kasagi, N., Tomita, T., Kuroda, K., 1992. Direct numerical simulation of passive scalar field in a turbulent channel flow. Trans ASME Journal of Heat Transfer 114, 598606.

Kawamoto, N., Kawamura, H., 1998. DNS and modelling of turbulent heat transfer in channel flow with a spanwise mean temperature gradient. In: 13th Australasian Fluid Mechanics Conference. Melbourne, Australia, pp. 611–614 (13–18 December).

Kawamoto, N., Kawamura, H., 1999a. DNS of turbulent heat transfer in a channel flow for different thermal boundary conditions. Transaction of JSME 65 (637), 181–188.

Kawamoto, N., Kawamura, H., 1999b. Turbulent heat flux model in consideration of Reynolds and Prandtl number effects. Transaction of JSME 65 (638), 194–202.

Kawamura, H., Abe, H., 2002. DNS of turbulent scalar transport in a channel flow up to $Re_\tau = 640$ with $Pr = 0.025$ and 0.71. In: Seventh TRA Conference. Seoul Nat'l Univ., Seoul, Korea, pp. 65–79 (27 April).

Kawamura, H., Abe, H., Matsuo, Y., 1999. DNS of turbulent heat transfer in channel flow with respect to Reynolds and Prandtl number effects. International Journal of Heat and Fluid Flow 20, 196–207.

Kawamura, H., Abe, H., Matsuo, Y., 2004. Very large-scale structures observed in DNS of turbulent channel flow with passive scalar transport. In: 15th Australasian Fluid Mechanics Conference. Sydney, Australia (13–17 December).

Kawamura, H., Abe, H., Shingai, K., 2000. DNS of Turbulence and Heat Transport in a Channel Flow with Different Reynolds and Prandtl Numbers and Boundary Conditions. pp. 15–32.

Kawamura, H., Kawamoto, N., Abe, H., Matsuo, Y., Yamamoto, K., 1998a. DNS and modeling of turbulent heat transfer in channel flow with various Prandtl numbers. In: 11th International Heat Transfer Conference, vol. 4. Kyongju, Korea, pp. 193–198 (23–28 August).

Kawamura, H., Ogawa, S., 2001. A consideration on linearity of passive scalar transport based on DNS of turbulent heat transfer in channel flow. In: Turbulent Heat Transfer III. Girdwood, Alaska 99587 (18–22 March).

Kawamura, H., Ohsaka, K., Abe, H., Yamamoto, K., 1998b. DNS of turbulent heat transfer in channel flow with low to medium-high Prandtl number fluid. International Journal of Heat and Fluid Flow 19 (5), 482–491.

Kawamura, H., Ohsaka, K., Yamamoto, K., 1997. DNS of turbulent heat transfer in channel flow with low to medium-high Prandtl number fluid. In: 11th Symposium Turbulent Shear Flows, vol. 1. Grenoble, pp. 8.7–8.12.

Kim, J., Moin, P., 1989. Transport of Passive Scalars in a Turbulent Channel Flow, vol. VI. Springer-Verlag, pp. 85–96.

Kim, K.C., Adrian, R.J., 1999. Very large-scale motion in the outer layer. Physics of Fluids 11 (2), 417–422.

Kozuka, M., Seki, Y., Kawamura, H., 2009. DNS of turbulent heat transfer in a channel flow with a high spatial resolution. International Journal of Heat and Fluid Flow 30 (3), 514–524 (the Seventh International Symposium on Engineering Turbulence Modelling and Measurements, ETMM7).

Lyons, S.L., Hanratty, T.J., McLaughlin, J.B., 1991. Direct numerical simulation of passive heat transfer in a turbulent channel flow. International Journal of Heat and Mass Transfer 34 (4-5), 1149–1161.

Marusic, I., McKeon, B.J., Monkewitz, P.A., Nagib, H.M., Smits, A.J., Sreenivasan, K.R., 2010. Wall-bounded turbulent flows at high Reynolds numbers: recent advances and key issues. Physics of Fluids 22 (6), 065103.

Matsubara, K., Kobayashi, M., Maekawa, H., 1998. Direct numerical simulation of a turbulent channel flow with a linear spanwise mean temperature gradient. International Journal of Heat and Mass Transfer 41 (22), 3627–3634.

Matsubara, K., Kobayashi, M., Maekawa, H., 1999. Direct numerical simulation of a turbulent channel flow with a linear spanwise nonuniformity of time–mean temperature (examination of the turbulence statistics). Heat Transfer – Asian Research 28 (8), 675–686.

Matsubara, K., Kobayashi, M., Sakai, T., Suto, H., 2001. A study on spanwise heat transfer in a turbulent channel flow – education of coherent structures by a conditional sampling technique. International Journal of Heat and Fluid Flow 22 (3), 213–219.

Monty, J.P., Stewart, J.A., Williams, R.C., Chong, M.S., 2007. Large-scale features in turbulent pipe and channel flows. Journal of Fluid Mechanics 589, 147–156.

Na, Y., Hanratty, T., 2000. Limiting behavior of turbulent scalar transport close to a wall. International Journal of Heat and Mass Transfer 43 (10), 1749–1758.

Na, Y., Papavassiliou, D.V., Hanratty, T., 1999. Use of direct numerical simulation to study the effect of Prandtl number on temperature fields. International Journal of Heat and Fluid Flow 20, 187–195.

Naguib, A.M., Wark, C.E., 1992. An investigation of wall-layer dynamics using a combined temporal filtering and correlation. Journal of Fluid Mechanics 243, 541–560.

Piller, M., 2005. Direct numerical simulation of turbulent forced convection in a pipe. International Journal for Numerical Methods in Fluids 49, 583–602.

Piller, M., Nobile, E., Hanratty, T.J., 2002. DNS study of turbulent transport at low Prandtl numbers in a channel flow. Journal of Fluid Mechanics 458, 419–441.

Redjem-Saad, L., Ould-Rouiss, M., Lauriat, G., 2007. Direct numerical simulation of turbulent heat transfer in pipe flows: effect of Prandtl number. International Journal of Heat and Fluid Flow 28 (5), 847–861.

Saha, S., Chin, C., Blackburn, H., Ooi, A., 2010. Numerical study of heat transfer in a fully developed turbulent pipe flow. In: 17th Australasian Fluid Mechanics Conference. Auckland, New Zealand (5–9 December).

Satake, S., Kunugi, T., Himeno, R., 2000. High Reynolds number computation for turbulent heat transfer in a pipe flow. In: High Performance Computing, Third International Symposium. Tokyo, Japan, pp. 514–523.

Seki, Y., Abe, H., Kawamura, H., 2003a. DNS of turbulent heat transfer in a channel flow with different thermal boundary conditions. In: 6th ASME–JSME Thermal Engineering Joint Conference, USA (16–20 March).

Seki, Y., Iwamoto, K., Kawamura, H., 2006. Prandtl number effect on turbulence quantities through high spatial resolution DNS of turbulent heat transfer in a channel flow. Dubrovnik, Croatia, Ch. Fifth Int. Symp. on Turbulence, Heat and Mass Transfer, pp. 301–304 (25–29 September).

Seki, Y., Kawamoto, N., Kawamura, H., 2003b. Proposal of Turbulent Heat Flux Model with Consideration of Linearity and Its Application to Turbulent Channel Flow with Various Thermal Boundary Condition, pp. 569–576.

Seki, Y., Kawamura, H., 2004a. DNS of turbulent heat transfer in a channel flow with a streamwisely varying thermal boundary condition. In: 15th Australasian Fluid Mechanics Conference. Sydney, Australia (13–17 December).

Seki, Y., Kawamura, H., 2004b. Turbulent heat flux model satisfying the linearity principle applied to the turbulent channel flow with various heating conditions. In: 1st International Forum on Heat Transfer. Kyoto, Japan, pp. 197–198 (24–26 November).

Seki, Y., Kawamura, H.,2005. DNS of turbulent heat transfer in a channel flow with streamwisely varying thermal boundary condition. In: Sixth KSME–JSME Thermal and Fluids Engineering Conference. Jeju, Korea (20–23 March).

Seki, Y., Kawamura, H., 2006. DNS of turbulent heat transfer in a channel flow with a varying streamwisely thermal boundary condition. Heat Transfer – Asian Research 35 (4), 265–278.

Tennekes, H., Lumley, J., 1972. A First Course in Turbulence. MIT Press Design Department, Cambridge, MA.

Tsukahara, T., Seki, Y., Kawamura, H., Tochio, D., 2004. DNS of turbulent heat transfer in a channel flow at very low Reynolds numbers. In: 1st International Forum on Heat Transfer. Kyoto, Japan, pp. 195–196 (24–26 November).

Yamamoto, Y., Kunugi, T., Tsuji, Y., 2009. Effects of Very-large Scale Structures in a High-Reynolds Turbulent Channel Flow on Medium-high Prandtl Number Heat Transfer, pp. 1–7.